Picosecond excitation and selective intramolecular rates in supersonic molecular beams. II. Intramolecular quantum beats and IVR

W. R. Lambert,[a] P. M. Felker,[b] and A. H. Zewail[c]
Arthur Amos Noyes Laboratory of Chemical Physics,[d] California Institute of Technology, Pasadena, California 91125

(Received 23 November 1983; accepted 27 April 1984)

An account of observations pertinent to quantum beat-modulated fluorescence decays of jet-cooled anthracene excited to $S_1 + 1380\ cm^{-1}$ is given. Based on both spectral and temporal characteristics of the beats, combined with theoretical expectations of such characteristics, it is shown that the interference phenomenon arises from the coupling of zero-order vibrational levels within the S_1 manifold. (Consistent with this interpretation is the observed absence of a magnetic field effect on the beats.) As such, it is shown to be a manifestation of restricted IVR. The results of measurements of rotational band contours and the effect of carrier gas on beat parameters are used to assess the role of rotations in the coupling between vibrational levels. Specific vibration–vibration coupling schemes are briefly discussed within the context of the observations.

I. INTRODUCTION

In a previous communication,[1] we reported preliminary results on the observation of intramolecular quantum beats in the time-resolved fluorescence of jet-cooled anthracene upon picosecond excitation to S_1, the first excited singlet manifold. It was apparent at that time that the phenomenon in anthracene differed in several respects from quantum interference effects observed in atoms[2] or in small molecules.[3] Even as the number of molecules found to exhibit quantum beats in their luminescence decays[4] has increased, these differences remain. In particular, a first point of difference is that anthracene has many degrees of freedom, and the density of levels is relatively high. Because of this and the anticipated role of rotations some theorists have actually predicted that beats should not be observable in such large molecules. A second, more important difference resides in the spectral characteristics of the molecular states giving rise to the beats. In all examples of molecules (except anthracene) exhibiting field-free quantum beats, there is no need to spectrally resolve the emission to observe beats. In anthracene this is definitely not the case since the modulation (or lack thereof) of fluorescence decays depends markedly on detection wavelength and bandwidth.

The fact that anthracene seems to be a case apart from other molecules that show quantum interference effects suggests differences in the nature of the states giving rise to the beats. Beats in other molecules can be explained by invoking the coupling of one optically active *electronic* state manifold with a different, optically dark manifold. Such an interelectronic state coupling scheme cannot easily accommodate the spectral characteristics of beats in anthracene. Instead, the coupling of rovibrational levels within one electronic manifold more naturally explains the spectral specificity associated with anthracene beats. The ability to observe the manifestations of such coupling in a large molecule like anthracene is quite important with regard to obtaining knowledge of the factors which influence intramolecular vibrational-energy redistribution (IVR).

In what follows, we give a full account of our earlier communication. Specifically, we present results on the following: (i) the detection and excitation energy dependence of the beats; (ii) the rotational involvement; (iii) the absence of a magnetic field effect; (iv) the effect of carrier gases; and (v) the effect of deuterium substitution. The data reinforce the interpretation that the beats observed in anthracene arise from coupled rovibrational levels within the S_1 manifold. In addition, the results clearly show both the involvement of rotational levels in the coupling which gives rise to the beats, and more importantly, the *real time* evolution of vibrational states undergoing restricted IVR. This paper is devoted to observations made at $1380\ cm^{-1}$ of excess energy although, as discussed later, beats have also been observed at many other vibrational excitations in S_1.

II. THEORETICAL

A. Field-free quantum beats

Before considering in detail the specific results for anthracene, it is useful to briefly consider some characteristics of field-free quantum beats in isolated molecules. The phenomenon of interest is a manifestation of the coherent superposition of excited molecular eigenstates

$$\psi = \sum_i a_i |e_i\rangle\, e^{-iE_i t/\hbar},$$

which can interfere amongst themselves upon radiative decay. One may note the following points:

(i) The type of interference phenomenon considered in this paper is intramolecular in nature. (Intermolecular beats in optical luminescence decays are possible, but to be observed require extremely difficult-to-achieve experimental conditions.[2]) One consequence of this is that Doppler effects do not influence the beats. A second consequence is that the beat frequencies ω_{ij}, which are indicative of interferences between pairs of states $|e_i\rangle$ and $|e_j\rangle$ separated by energy $E_{ij} = \hbar\omega_{ij}$, contain information regarding the excited state level structure *only*.[2]

(ii) The form of the beat-modulated decay need not de-

[a] Present address: Bell Laboratories, 600 Mountain Avenue, Murray Hill, New Jersey 07974.
[b] IBM Research Fellow.
[c] Camille and Henry Dreyfus Foundation Teacher–Scholar.
[d] Contribution No. 6896.

 0021-9606/84/172217-16$02.10

pend on excitation (or detection) direction or polarization,[5] in contrast to atomic systems.[2]

(iii) To create the superposition state ψ, it is necessary that all $|e_i\rangle$ have nonzero transition moments connecting them by absorption to the same ground state $|g\rangle$. This imposes stringent conditions on the states which can contribute to ψ, especially in a molecule of high symmetry like anthracene.

(iv) Given that point (iii) is fulfilled, beats can occur on the decay of the resonance fluorescence (i.e., $\psi \rightarrow |g\rangle$). In addition, beats can occur for the emission to other ground state levels $|f\rangle$, if at least two of the $|e_i\rangle$ states in ψ have nonzero transition moments connecting them to a particular $|f\rangle$.

The above points are fundamental to the analysis of beats in anthracene. Much of what follows implicitly assumes their validity.

B. Intramolecular couplings and quantum beat signals: The concept of phase-shifted beats (Ref. 6)

Coupling within an optically accessible manifold (electronic transition moment to the ground state $\neq 0$) is a qualitatively different situation than S_1-triplet or S_1–S_0 coupling. In the first situation, all zero-order levels involved have nonnegligible transition moments to at least some ground state levels. This is not true, however, for the latter schemes. As we shall show in this section, this difference can lead to observable consequences regarding the spectral dependence and phase shifts of quantum beats. First, we derive expressions for quantum beat signals arising from coupled two-level systems subject to varying constraints. A level scheme pertinent to this analysis is given in Fig. 1. We then briefly consider the case of multilevel systems. The results derived[6] are eventually used in Sec. V to interpret observations made on anthracene.

Consider, first, the following expression for the fluorescence signal[2] $S(t)$ representing excitation (see Fig. 1) from a ground state level $|g\rangle$ to excited states $|e_1\rangle$ and $|e_2\rangle$, with subsequent emission to the ground state levels $|f\rangle$ (note that these states are taken to be molecular eigenstates):

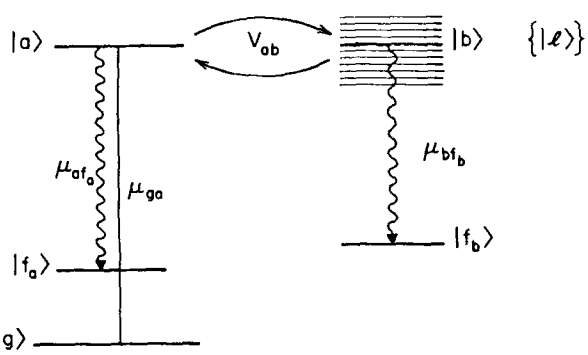

FIG. 1. A level structure schematic pertaining to the theoretical discussion of Sec. II B. Only the zero-order S_1 level $|a\rangle$ has any absorption strength from the initially populated S_0 level $|g\rangle$. $|a\rangle$ is coupled to one state $|b\rangle$ in the S_1 manifold of states $\{|l\rangle\}$. This coupling produces eigenstates $|e_1\rangle$ and $|e_2\rangle$ (not shown). Quantum beat behavior depends on the nature of $|b\rangle$ and on the nature of the fluorescence band(s) detected.

$$S(t) = K \sum_f \sum_{i,j=1}^{2} \langle e_i|\hat{e}_0\cdot\hat{\mu}|g\rangle\langle g|\hat{e}_0^*\cdot\hat{\mu}|e_j\rangle \times \langle e_j|\hat{e}_d\cdot\hat{\mu}|f\rangle\langle f|\hat{e}_d^*\cdot\hat{\mu}|e_i\rangle e^{-\Gamma t} e^{-i\omega_{ij}t}, \quad (1)$$

where $\hat{e}_0$ and $\hat{e}_d$ are the excitation and detection polarizations, $\hat{\mu}$ is the transition electric dipole operator, Γ is the decay rate of $|e_1\rangle$ and of $|e_2\rangle$, $\omega_{ij} = (E_i - E_j)/\hbar$, and K is a constant. Now, take $|e_1\rangle$ and $|e_2\rangle$ to be the states that result from the coupling of the zero-order states $|a\rangle$ and $|b\rangle$:

$$|e_1\rangle = \alpha_{1a}|a\rangle + \alpha_{1b}|b\rangle,$$
$$|e_2\rangle = \alpha_{2a}|a\rangle + \alpha_{2b}|b\rangle, \quad (2)$$

where all the coefficients are real, where $\alpha_{1a}(\equiv\alpha) = -\alpha_{2b}$ and $\alpha_{2a}(\equiv\beta) = \alpha_{1b}$, and where $\alpha_{ia}^2 + \alpha_{ib}^2 = 1$. Using the definition $\langle m|\hat{e}\cdot\hat{\mu}|n\rangle \equiv \mu_{mn}$, where m can be a or b, and n can be g or f:

$$S(t) = K \sum_f \sum_{i,j=1}^{2} (\alpha_{ia}\mu_{ag} + \alpha_{ib}\mu_{bg}) \times (\alpha_{ja}\mu_{ag}^* + \alpha_{jb}\mu_{bg}^*)(\alpha_{ja}\mu_{af} + \alpha_{jb}\mu_{bf}) \times (\alpha_{ia}\mu_{af}^* + \alpha_{ib}\mu_{bf}^*) e^{-\Gamma t} e^{-i\omega_{ij}t}. \quad (3)$$

(Note that we have suppressed any reference to light polarization.) We shall consider three limiting cases[6] of Eq. (3):

The first case [case (1)] corresponds to singlet–triplet or S_1–S_0 coupling, and involves taking $|a\rangle$ as optically accessible and $|b\rangle$ as optically dark. In other words: $\mu_{ag}, \mu_{af} \neq 0$ for at least some f; and $\mu_{bg} = \mu_{bf} = 0$ for all f. The fluorescence signal of Eq. (3) for case (1) becomes

$$S(t) \equiv S_1(t) = K \sum_f |\mu_{af}|^2 |\mu_{ag}|^2 e^{-\Gamma t} \times (1 - 2\alpha^2\beta^2 + 2\alpha^2\beta^2 \cos\omega_{12}t), \quad (4)$$

where we have used the definitions for α and β, and the fact that $\alpha^2 + \beta^2 = 1$. Note that the sign of the interference term is positive and that the time dependence of the signal does not depend upon detection of the transition to a particular f. These points shall be very important in showing the inapplicability of interelectronic state coupling schemes to anthracene beats.

The second case [case (2)] is somewhat similar to case (1) in that only the $|a\rangle$ state is assumed to provide the absorption and emission strength of the excited states $|e_i\rangle$. The difference from case (1) is that now we assume that only one band in the dispersed fluorescence spectrum is detected. This corresponds to limiting the summation over f in Eq. (4) to one value f_a. This has no effect on the time behavior of the fluorescence signal: $S_2(t) \sim S_1(t)$. Unlike case (1), however, case (2) can arise in the coupling of two vibrational levels of the same electronic state, as we shall see below.

The third case [case (3)] corresponds to the situation wherein $|a\rangle$ alone has absorption strength from $|g\rangle$, but that conditions are such that the only detected emission band corresponds to a transition which gains its strength from $|b\rangle$ (i.e., a transition of the form $\psi_{ex} \rightarrow |f_b\rangle$, where $|f_b\rangle$ can combine with $|b\rangle$ but not with $|a\rangle$). In this case, $\mu_{ag}, \mu_{bf_b} \neq 0$; and $\mu_{bg} = \mu_{af_b} = 0$. Equation (3) for case (3) becomes

$$S(t) \equiv S_3(t) = 2Ke^{-\Gamma t}\alpha^2\beta^2|\mu_{ag}|^2|\mu_{bf_b}|^2\{1 - \cos\omega_{12}t\}. \quad (5)$$

It is clear that $S_3(t)$ involves a 180° phase shift in its quantum interference term relative to $S_1(t)$ and $S_2(t)$. Moreover, one may see that it is necessary to restrict the emission that is detected to observe this phase shift. For, the band corresponding to $\psi_{ex} \rightarrow |g\rangle$ also occurs in the emission spectrum (as, probably, do other bands deriving their emission strength from $|a\rangle$). The modulations on the decay of this band, if it is not eliminated from being detected, will destructively interfere with those of the case (3) band, and this will tend to wash out the beats of the detected decay.

As the above discussion of case (3) shows, case (2) and case (3) bands can both be present in the same dispersed fluorescence spectrum. Such a situation arises when an optically active vibrational level $|a\rangle$ couples with another vibrational level $|b\rangle$ that cannot be reached in absorption from the S_0 vibrationless level. The optically active level solely determines the absorption strength to the molecular eigenstates. However, the emission spectrum is determined by the different Franck–Condon factors for emission of the $|a\rangle$ and $|b\rangle$ zero-order levels. As a result, both case (2) and case (3) bands can exist. Both types of bands are characterized by a beat pattern having the same frequency ω_{ij}. *However, they are distinguishable, not only by the phase of the beat pattern, as mentioned above, but also by the degree of modulation of the beats.*[6] For, one can see by consideration of $S_2(t)$ and $S_3(t)$ that the modulation depth in case (2) is coupling dependent ($= 2\alpha^2\beta^2/1 - 2\alpha^2\beta^2$) and, in general, is less than 100%, whereas the modulation in case (3) is always 100%.

C. Multilevel systems

In large molecules, a two-level model for vibrational coupling is obviously an approximation to the actual situation. This is so because (a) each coupled vibrational level has its own rotational manifold, and (b) the possibility exists that more than two vibrational levels are mutually coupled. The characteristics which both these kinds of multilevel situations can exhibit in beat-modulated fluorescence decays will be dealt with in greater detail in subsequent publications.[7] It is sufficient for our purpose here to briefly consider how simple two-level decays [Eqs. (4) and (5)] may be modified by multilevel effects.

1. Rotational level structure

The coupling of two rovibrational manifolds can be viewed in terms of an ensemble of two-level systems. This simplification arises from rotational selection rules for vibrational coupling. Because of this, the results of Sec. II B are valid for each pair of rotational levels coupled between two manifolds. However, under typical experimental conditions a fluorescence decay contains contributions from a number of rotational levels. Since there may be variations in coupling with rotational level, one expects a distribution of beat frequencies to contribute to any given experimental decay. Obviously, such a distribution will modify the two-level results of Sec. II B. For instance, observed modulation depths may be less than those predicted by a two-level model. Or, a number of distinguishable beat frequencies may occur in the decay of any given fluorescence band. It turns out that rotational level effects have, indeed, been observed for anthracene, as will be detailed below and elsewhere.[7]

2. Multilevel coupling

Another generalization of the two-level system of Sec. II B involves the possibility of coupling between three or more rovibrational manifolds. Such multilevel coupling has both spectral and temporal consequences which are different from those of a two-level system. For instance, three coupled vibrational levels would be expected to give rise to a least three different kinds of fluorescence bands, each with decays modulated at the same three beat frequencies (two of which add to give the third) but distinguished by different phases and amplitudes of the modulation components. While there are no results presented in this paper which represent definitive evidence for multilevel coupling of this sort, this does not preclude the possibility that such a situation does indeed obtain in anthracene but that we do not have the experimental capability (e.g., time resolution) to observe its manifestations. Hence, deviations that our experimental results may make from the theoretical expectations of Sec. II B (deviations such as less than predicted modulation depths or more than two kinds of fluorescence bands, etc.) could be due, in part, to hidden effects of multilevel coupling. [See note added in proof].

D. Quantum beats and IVR

It is now pertinent to consider what information quantum beats can give us concerning IVR processes. Let us first establish a link between beats and IVR by again considering the coupled two-level vibrational system of Sec. II B. Assuming absorption strength due entirely to $|a\rangle$, δ-function excitation at $t = 0$ prepares a superposition state:

$$|\psi_{ex}(t)\rangle \sim [\alpha^2|a\rangle e^{-iE_1t/\hbar} + \beta^2|a\rangle e^{-iE_2t/\hbar} + \alpha\beta|b\rangle e^{-iE_1t/\hbar} - \alpha\beta|b\rangle e^{-iE_2t/\hbar}]e^{-\Gamma t/2}. \quad (6)$$

Now at $t = 0$: $\psi_{ex}(0) \sim |a\rangle$; while at $t > 0$, $\psi_{ex}(t)$ contains contributions from $|b\rangle$. Clearly, then, there is an evolution in time of the zero-order vibrational level content of $\psi_{ex}(t)$. It is instructive to calculate the contributions of $|a\rangle$ and $|b\rangle$ to $\psi_{ex}(t)$:

$$|\langle a|\psi_{ex}(t)\rangle|^2 \sim e^{-\Gamma t}(1 - 2\alpha^2\beta^2 + 2\alpha^2\beta^2\cos\omega_{12}t), \quad (7a)$$

$$|\langle b|\psi_{ex}(t)\rangle|^2 \sim e^{-\Gamma t}(2\alpha^2\beta^2)\{1 - \cos\omega_{12}t\}. \quad (7b)$$

Equations (7a) and (7b) are of the same form as $S_2(t)$ and $S_3(t)$, respectively (Sec. II B). Thus, it is apparent that fluorescence decays of case (2) bands probe the $|a\rangle$ content of the excited state ψ_{ex}, and the decays of case (3) bands probe the $|b\rangle$ content. Within the context of vibration–vibration coupling, the phase shift of case (3) bands actually represents a characteristic time for energy flow into the $|b\rangle$ vibration. The modulation depth of case (2) bands is a direct indication of the completeness of energy transfer. The limited scope of the redistribution (only two vibrational levels involved) is indicated by the finite recurrence time $2\pi/\omega_{12}$ (i.e., the quasiperiodic behavior.[6])

III. EXPERIMENTAL PROCEDURES

A. Jet-beam system

The 36×12 in. cylindrical stainless steel chamber was evacuated with a 12 in. bore, ring jet booster diffusion pump (Edwards 18B4A) with a pumping speed of 4000 l/s ($<10^{-2}$ Torr). The diffusion pump was backed with a 150 CFM roughing pump (Kinney KT-150). The ultimate pressure obtained with this system is 10^{-5} Torr. Under normal operating conditions, (e.g., a 150 μ pinhole at 3 atm back pressure of nitrogen) the chamber pressure was less than 10^{-3} Torr. The diffusion pump was not baffled in order to take full advantage of the maximum throughput. The vacuum chamber could be isolated from the pumping system with a pneumatically actuated right angle valve (Vac-U-Torr Products) in order to provide access to the chamber between experiments.

On the beam chamber 6 in. ports, which were covered with either plexiglass or quartz windows, provided convenient access to the nozzle assembly and enabled efficient fluorescence collection. Insert flanges enabled moving the fluorescence collection window to within 1.5 in. of the horizontally mounted, easily translatable nozzle assembly. Laser beams passed vertically through 20 in. long entrance and exit baffles which reduced scattered laser light.

B. Materials and expansion conditions

H_{10}-anthracene (Aldrich) and d_{10}-anthracene (Aldrich) were zone refined (100 passes) prior to use. In some experiments, unpurified h_{10}-anthracene (Aldrich, $>98\%$ purity) was used. Differences in the results obtained with purified and unpurified samples were not observed. $9d_1$-anthracene and $9,10d_2$-anthracene were synthesized by acid catalyzed deuterium–hydrogen exchange[8] from the respective brominated precursors, 9-bromoanthracene (Aldrich) and 9,10-dibromoanthracene (Kodak). Purification was accomplished upon repeated recrystallization from $CHCl_3$. The isotopic purity of $9,10d_2$- and $9d_1$-anthracene was determined by mass spectral analysis to be $>95\%$.

In order to introduce the compounds into the free jet expansions, samples were contained in cylindrical Pyrex nozzles, which were tapered at one end to produce pinhole openings of 50–200 μm into the vacuum chamber. Specific conditions are given with the experimental observations. Pyrex nozzles were used because of the following advantages over stainless steel nozzles and metal pinholes: Organic compounds do not readily decompose on Pyrex surfaces at high temperatures, the ability to view Pyrex nozzle tips allows easy assessment of the possibility of clogged pinholes, and Pyrex nozzles are easily cleaned. The samples were heated to 150–180 °C. Slightly higher temperatures were maintained at the nozzle tip to prevent clogging.

Helium, neon, and nitrogen at pressures up to 10 atm were used as carrier gases. Preliminary experiments with argon indicated a strong propensity for complex formation, and, as a consequence, argon was not used. Vacuum chamber pressure was continuously monitored either with an ionization or convectron gauge. Typical values for X/D, where X is the nozzle to laser distance and D the nozzle pinhole diameter, were >30. The assessment of the effects of intermolecular collisions on the results reported here was made by varying X and determining any changes in results. In no case was any substantial effect observed for helium or neon, as X/D was increased beyond 30. On the other hand, the use of nitrogen was found to produce dispersed fluorescence bands consistent with the vibrational relaxation of S_1 anthracene via intermolecular interactions. This effect was determined to be entirely unrelated to quantum beats (by taking fluorescence decays at various values of X/D), but was found to produce some minor differences in dispersed fluorescence spectra obtained in N_2 expansions vs those obtained in He and Ne expansions. A discussion of the influence of the expansion conditions on the cooling of anthracene may be found in Ref. 9.

C. Picosecond laser system

For energy resolved fluorescence and time-resolved measurements, excitation was provided by a synchronously pumped, mode-locked, cavity-dumped picosecond dye laser system. A mode-locked argon ion laser (Spectra Physics 171) at 1 W average power pumped the dye laser to generate 15 ps pulses with a bandwidth of 2 Å. The average power per pulse was 30 nJ. The repetition rate of the cavity-dumped picosecond pulses was variable and normally operated at 4 MHz. The extinction ratio between the dumped and nondumped pulses was on the order of 500:1. The laser pulse duration (15–200 ps) and bandwidth (5.0–0.4 Å) could be varied by the insertion of various intracavity dye laser tuning elements (wedge, three-plate birefringent filter, fine tuning etalon, and solid etalon). The laser dyes DCM and R6G (Exciton) were used to generate tunable laser power from 7400 to 5700 Å. The determination of the laser bandwidth was made with a scanning monochromator (0.25 Å resolution).

Precise mode locking of the dye laser (accomplished by matching the argon ion laser and dye laser cavity lengths) was necessary in order to achieve minimum pulse widths and maximum laser power. Approximate alignment could be determined by monitoring the average UV power produced by second harmonic generation. Fine adjustment was accomplished by maximizing the autocorrelation intensity.

The measurement of the temporal characteristics of the laser pulse was accomplished using zero background second harmonic generation. The dye laser beam was separated into two parts, the length for one of which was variable. The two noncollinear beams were focused onto a 0.2 mm thick $LiIO_3$ crystal to generate the second harmonic. A stepper motor-driven translation stage was used to vary the time delay between the arrival of the two pulses. The second harmonic generation signal for this arrangement is proportional to the autocorrelation function of the pulse intensity. The second harmonic was detected with a filtered photomultipler tube. Phase sensitive detection was used to provide a large dynamic response range. The output of the lock-in amplifier (PAR HR-8) was digitized with a voltage to frequency converter and temporarily stored in a multichannel analyzer (MCA). The contents of the MCA were transferred to a PDP 11/23 computer for subsequent analysis. Typical results are shown in Fig. 2. Details for the analysis of pulse width and coherence time can be found in Ref. 10.

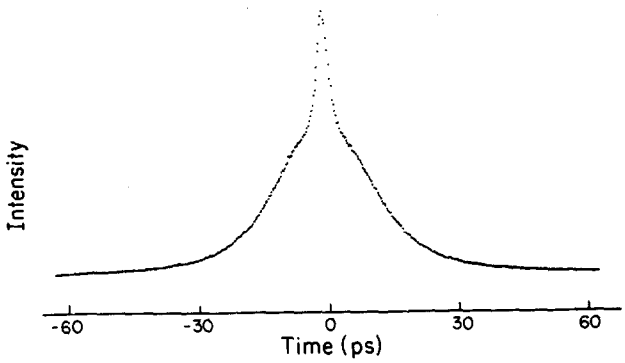

FIG. 2. An example of an autocorrelation trace of the pulsed output from the picosecond dye laser. The laser is not optimally mode locked in order to emphasize the coherent spike and the envelope of the pulse. The width of the pulse envelope derived from this trace is ~30 ps.

For the purposes of investigating the dynamics of anthracene, the second harmonic of the picosecond dye laser was generated using 1 cm^3 phase matched lithium iodate crystals (Cleveland Crystals). Two crystals were required to produce tunable ultraviolet power over the range of interest: (i) a $LiIO_3$ crystal cut for the 6100 Å fundamental, and (ii) a $LiIO_3$ crystal cut for the 6900 Å fundamental. A 50 mm focal length lens focused the fundamental onto the doubling crystal to produce the second harmonic beam. Although the UV beam was elongated due to differences in the phase matching angle along the path of the tightly focused fundamental, maximum power was produced. The conversion efficiency was measured to be ~11%.

D. Picosecond/jet-beam arrangement

The arrangement for the picosecond-jet experiments is depicted schematically in Fig. 3. The second harmonic was collimated, directed through a 50 cm long entrance baffle provided with three adjustable apertures, and focused onto the free jet expansion downstream from the nozzle. The mirror which directed the laser beam through the free jet apparatus was antireflection coated, enabling the transmitted laser fundamental to be directed onto a fast photodiode which was then used to trigger the timing electronics. The laser beam exited the free jet expansion chamber through an additional 50 cm long light baffle.

Molecular fluorescence was collected with an $f/1$ lens and imaged with another lens onto the entrance slit of the monochromator. This simple two-lens system, although not maximizing the collection efficiency, allowed versatility in the optical alignment. Scattered light was not found to be a problem in these experiments. The emission was resolved with a microprocessor controlled, $f/6.9$, 0.5 m monochromator (Spex Industries 1870 and CD2 microprocessor) with a grating dispersion of 16 Å/mm.

The energy and time-resolved fluorescence measurements were made using single photon counting techniques. Emission was detected with an Amperex XP2020Q photomultiplier, and the output sent to a constant fraction differential discriminator (ORTEC model 583). To obtain the decay measurement an inverted operating configuration was used in which the fluorescence photon signal provided the start pulse for the time-to-amplitude conversion (TAC, ORTEC model 457). This configuration provided an optimal data acquisition rate.[11] The stop pulse to the TAC was generated from the laser fundamental by means of a fast photodiode and a constant fraction discriminator. The ratio of the photon detection rate to the laser repetition rate was always less than 1%. The output of the TAC was processed and temporarily stored in an MCA used in the pulse height analyzer mode. The time base was calibrated using the full laser repetition rate (82 MHz) based upon knowledge of the mode locking frequency. The instrument response function, obtained by scattering laser pulses from the nozzle, was found to be as narrow as 250 ps. (In recent experiments in this

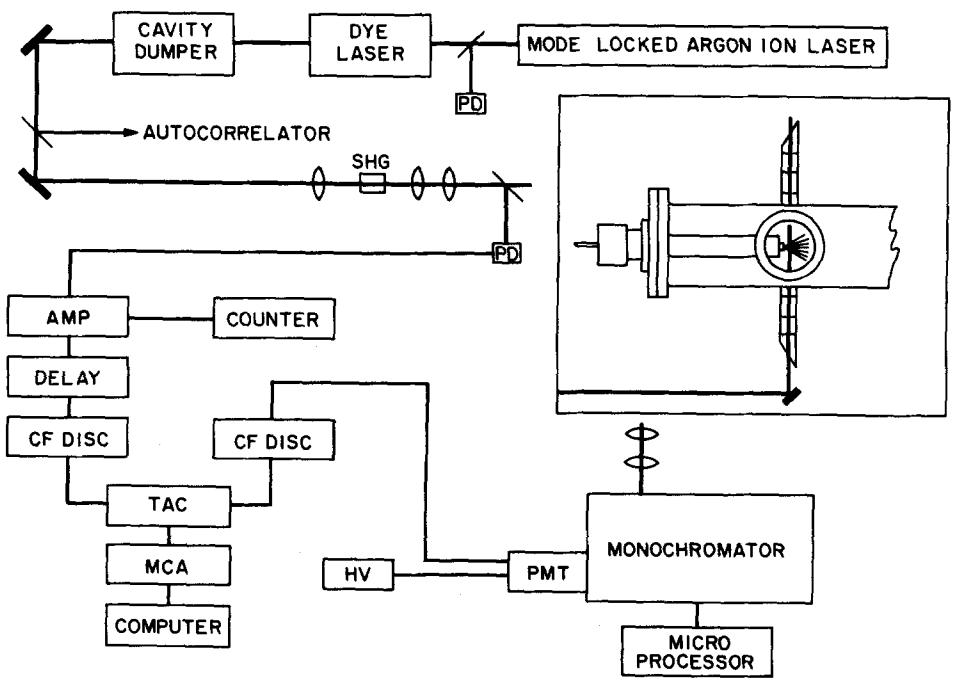

FIG. 3. A schematic of the picosecond-jet apparatus and detection electronics. Most symbols are self-explanatory, or are obvious from the text. "PD" represents photodiode. "SHG" is second harmonic generation.

laboratory,[7] our response function was ~70 ps, allowing for a time resolution of exponential decay of ~10 ps.) For collecting energy dispersed fluorescence spectra, PMT pulses were acquired by the MCA in multichannel scalar mode. All spectra which were accumulated on the MCA were subsequently transferred to a PDP 11/23 computer for analysis.

E. Fluorescence excitation spectra

A pulsed nitrogen pumped dye laser and a YAG pumped dye laser system were used to produce excitation spectra. For the nitrogen laser system, the spectral bandwidth and temporal pulse width were measured to be 0.5 cm^{-1} and 9 ns, respectively. The dye laser grating was scanned with an externally driven stepper motor. The absolute laser wavelength was calibrated using the optogalvanic method.[12] The second harmonic was generated by focusing the laser fundamental onto a 2 cm KDP crystal, the UV was then collimated, and subsequently focused onto the free jet expansion. Scattered light was reduced by passing the laser beam through baffles extending to either side of the expansion chamber. Fluorescence was collected with $f/1$ optics and passed through the monochromator before being focused onto the photomultiplier tube. By varying monochromotor slit widths and wavelength settings, we were able to obtain excitation spectra for detection of essentially total fluorescence as well as for the detection of selected fluorescence bands. The output of the photomultiplier was integrated with a boxcar averager (PAR 162/164). The averaged signal was digitized with a voltage-to-frequency converter and temporarily stored in a multichannel analyzer. The data were subsequently transferred to a PDP 11/23 computer for analysis. The fluorescence excitation spectra obtained with the nitrogen laser were not normalized to the laser pulse energy.

Using the YAG system, we obtained normalized excitation spectra by utilizing A/B boxcar integration. The entire system is described elsewhere[13] and no details will be given here.

F. Magnetic field experiments

The magnetic field was applied by means of a water cooled Helmholtz coil, calibrated using a Gaussmeter (Bell Model 610). Fields up to 200 G could be applied before magnet overheating became a problem. To verify the presence of a field, experimental results on pyrazine[4(a)] were reproduced using the same coil parameters that were used in the anthracene experiments.

G. Methods of analysis

1. Fluorescence lifetimes

Fluorescence decay curves which did not exhibit quantum beats were fit to a single exponential function of the form;

$$G(\tau) = A\, e^{-t/\tau} + B,$$

where A, B, and τ are adjustable parameters. For these cases the system response function was sufficiently short compared to the observed decay that analysis did not require deconvolution. The curve fitting was performed on a PDP 11/23 computer using a nonlinear least squares routine based on Marquardt's algorithm.[14] The quality of the fits was determined by the reduced chi squared (χ_ν^2),[14(b)] and by inspection of the weighted residuals and the residual autocorrelation function.[15]

2. Quantum beats

Fourier transform analysis was applied to the fluorescence decays which exhibited quantum beats. Spectra which exemplify the steps in the analysis of the quantum beats are shown in Fig. 4.

Direct Fourier transformation of decay data was found to produce frequency domain spectra dominated by half-

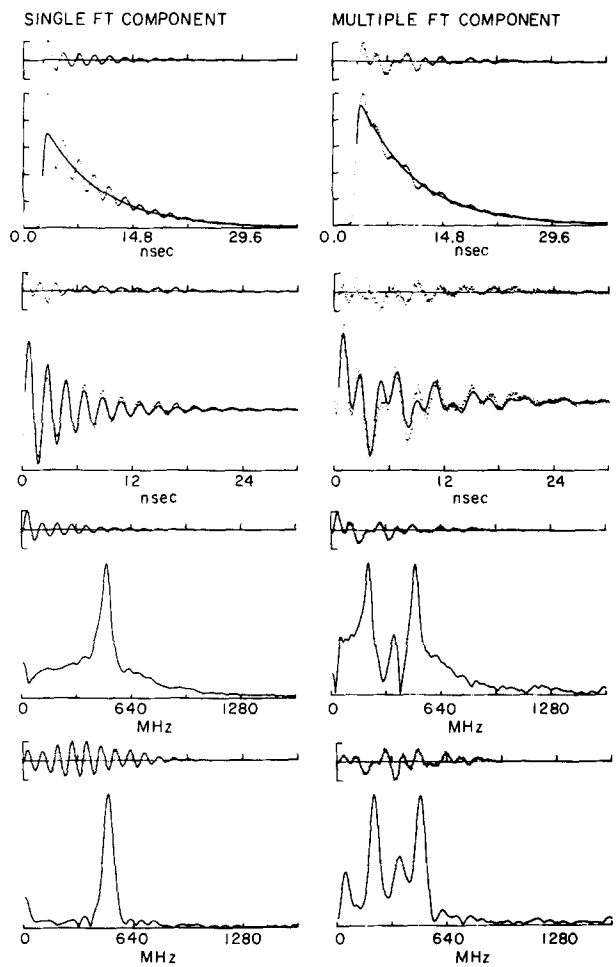

FIG. 4. Representative data presented for different stages of the analysis of fluorescence decays exhibiting one or a number of oscillatory components. (i) The top figures show the time-resolved fluorescence decay which contains both exponential and oscillatory compoonents. (ii) After subtraction of the single exponential component, the residual, which contains only damped oscillatory terms, is generated. The parameters determined upon direct Fourier transformation are compared to those obtained by fitting the residual to a sum of damped sinusoids. (iii) The residual is Fourier transformed to produce the frequency domain spectrum. (iv) Comparison of the spectrum obtained upon direct Fourier transformation of the residual with that obtained by first multiplying the residual with a Hanning window prior to transformation indicates the amount of leakage and sidelobe formation that results from the truncation of the residual waveform.

Lorentzians centered at zero frequency. Because of this, in order to accomplish analysis of the quantum beats, it was first necessary to remove unmodulated exponential terms from the decays. The response function of the system $F(t)$ was convoluted with an assumed single exponential decay function $G(t)$ to obtain

$$I(t) = \int_0^t dt' \, F(t')G(t-t') . \tag{8}$$

$I(t)$ was then fit to the experimental data by adjusting parameters in G. Curve fitting was performed beginning ten data points (760 ps) to earlier time than the maximum intensity. The best least squares fit[14] was then subtracted from the experimental data to produce a residual function composed only of damped oscillatory terms. Fourier transformation of the residual generated the frequency domain spectrum, which in turn was analyzed to determine physical parameters associated with the interference terms. Fourier transformation was accomplished using a routine based upon the Cooley–Tukey fast Fourier transform algorithm.[16]

When a single oscillatory term predominated, the Fourier transformation yielded frequency domain spectra which were relatively free of leakage and sidelobe interference. In these cases the spectral parameters of interest (peak position, FWHM, and area) were obtained upon fitting the single peak to a Lorentzian line shape profile. On the other hand, the situation regarding the Fourier transformation of the residuals exhibiting multiple interference terms is more problematic. The Fourier transforms of these residuals generally produced several apparently unsymmetrical peaks in the frequency domain. The extent to which sidelobes and leakage contributed to these spectra could be determined upon application of appropriate window functions to the data prior to transformation. The application of window functions[17] significantly removes sidelobes and leakage which result from the convolution of the rectangular sampling window in which the time domain data were acquired. The relative peak positions in the frequency domain are maintained, however, artifical line shapes are produced upon Fourier transformation, which are broader than they otherwise would be.[17,18] Application of a Hanning lag window[16(a),17] revealed that much of the asymmetry associated with the frequency domain peaks as the result of artifacts produced as the result of Fourier transformation of the truncated waveform. The frequency domain spectra generated from data to which the Hanning function had been applied therefore provided an indication of the number and relative positions of the peaks.

The validity of parameters obtained by Fourier analysis were verified by fitting the residual directly to a sum of damped sinusoids. The agreement of the values determined by the two methods was excellent.

In addition to Fourier analysis of beating decays, it was desirable in some instances to directly simulate the observed decays. An assumed oscillatory decay function was convoluted with a measured system response function to yield the calculated decay. Simulations of this sort were found to be useful in analyzing modulated decays for possible phase shift behavior.

IV. RESULTS

As in our preliminary report,[1] we shall be concerned in this paper with the characteristics of beat-modulated fluorescence decays that arise upon excitation of the strong band appearing at $S_1 + 1380(\pm 3)$ cm^{-1} in the h_{10}-anthracene excitation spectrum, a band which has been assigned as the 6_0^1 transition.[19] (Beats at other excitation wavelengths are reported in Ref. 6; see also note added in proof.) The results presented below are grouped in sections according to the effects they exemplify with regard to these beats.

A. The influence of detection wavelength and bandwidth

The observation of quantum beats in the fluorescence decay of 6_0^1-excited anthracene depends upon very specific detection conditions. In the dispersed fluorescence corresponding to this excitation (Fig. 5) some of the total number of bands that appear exhibit beat-modulated decays.[20] The bands which do exhibit resolvable beats (labeled in Fig. 5) show the same beat patterns for given excitation and jet conditions (under the particular conditions of the figure the dominant beat frequency is 490 MHz), but vary in the extent to which their decays are modulated (Fig. 6). From Fig. 6, it is apparent that the best modulated beats occur for detection corresponding to the band at a shift of 1125 cm^{-1} from the excitation energy. Consideration of other jet-cooled anthracene spectra[9,21] show that this band does not correspond to any obvious optically active fundamental, overtone, or combination band. (We shall argue below that this fact is not paticularly surprising.) Other moderately well-modulated decays occur for detection of the emission bands at shifts of 1518, 1910, and 2292 cm^{-1} (Fig. 6). These bands are readily assigned to a progression of the optically active 390 cm^{-1} $a_g(12)$ mode built upon the 1125 cm^{-1} transition. The bands at 0 and 390 cm^{-1}, corresponding to the transitions 6_0^1 and $6_0^1 12_1^0$, are less modulated than the other beating decays (Fig. 6).

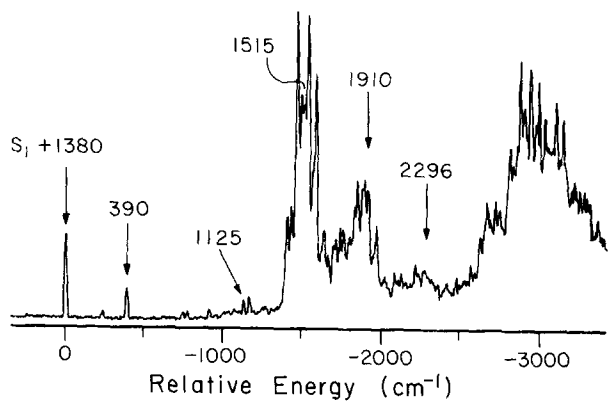

FIG. 5. Dispersed fluorescence spectrum of anthracene excited to $S_1 + 1380\,\text{cm}^{-1}$ (6_0^1). The energy scale of the figure is relative to the excitation energy (marked as $S_1 + 1380$). Scatter contributes minimally to the band at 0 cm^{-1}. Arrows mark those bands for which beats have been observed (Ref. 20). Experimental conditions: nozzle-to-laser distance ($\equiv X$) = 3 mm, nozzle pinhole diameter ($\equiv D$) = 100 μm, carrier gas pressure ($\equiv P$) = 30 psi He, laser bandwidth ($\equiv$BW) = 0.5 Å, monochromator resolution ($\equiv R$) = 1.6 Å, sample temperature ($\equiv T$) = 180 °C.

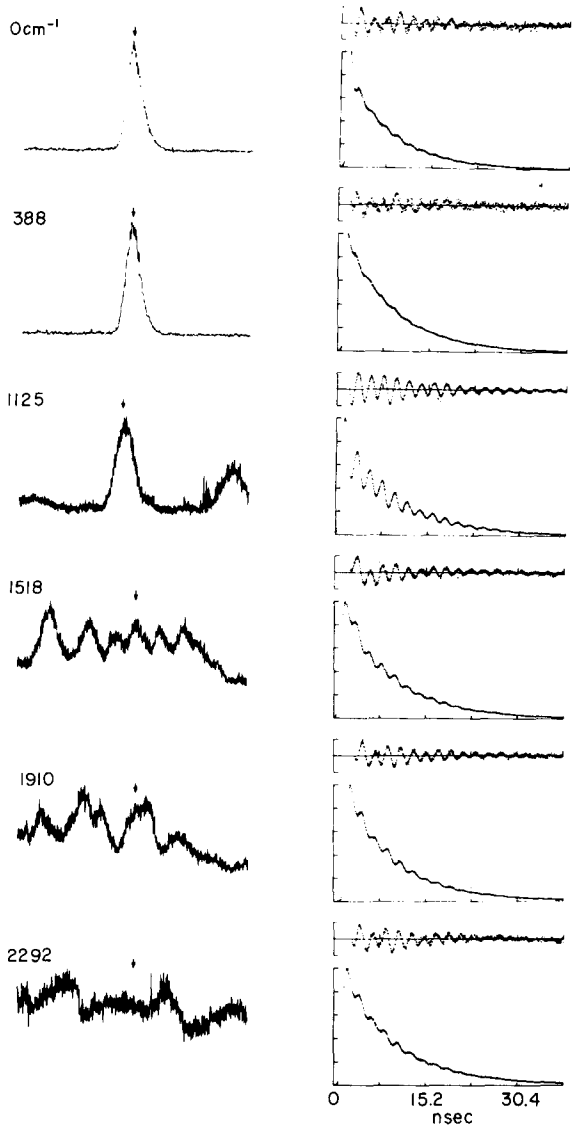

FIG. 6. The high resolution ($R = 0.3$ Å) energy resolved fluorescence spectra (each taken over a 10 Å range) of the transitions which exhibit quantum beats, and the corresponding time-resolved fluorescence decays. The transitions refer to those indicated in Fig. 5. The decays were taken with $R = 0.5$ Å. The residuals of the time-resolved spectra are normalized by the reciprocal of the number of counts so as to accentuate the oscillatory behavior. For all data: $X = 5$ mm, $D = 150\ \mu$m, $P = 45$ psi N_2, $T = 180$ °C.

A marked detection bandwidth effect on the decay modulation of the $1125 + n \times 390\ \text{cm}^{-1}$ bands ($n = 0,1,2,3$) has been observed. An example is given in Fig. 7 for the 1125 cm^{-1} band. Even larger effects occur for the other bands.[6] This influence of detection bandwidth reflects the presence of nonbeating[20] bands in the spectral vicinity of the beating transitions. One is led to expect from this that increases in modulation depth would be observed for the beating bands (particularly the ones at 1518, 1910, and 2292 cm^{-1}) if greater spectral resolution than that used to obtain the decays of Fig. 6 were experimentally feasible. In contrast, the 0 and 390 cm^{-1} bands appear in congestion-free regions of the fluorescence spectrum and do not exhibit comparable detection bandwidth effects.

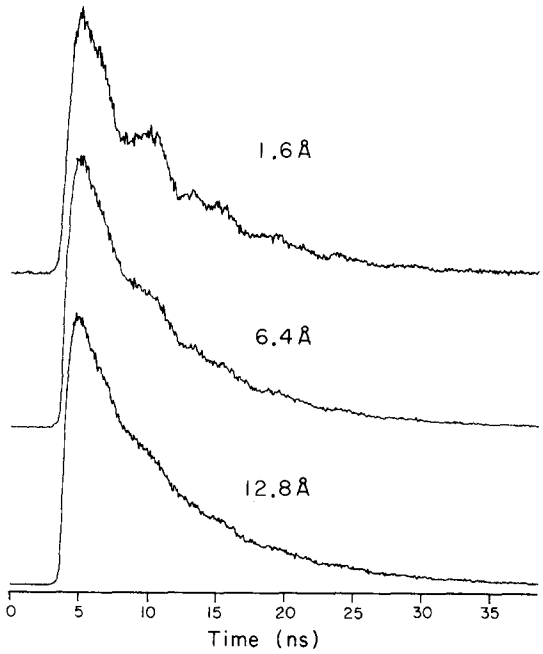

FIG. 7. The detection bandwidth effect on the decay of the 1125 cm^{-1} band in the 6^1 spectrum. R is given for each decay in the figure. For all decays: $X = 3$ mm, $D = 100\ \mu$m, $P = 45$ psi He, BW = 0.5 Å, $T = 180$ °C. Note that the decays were taken using helium expansions and that they are therefore different than the decays of Fig. 6 (N_2 expansion). Beat modulated decays obtained using N_2 expansions also exhibit a clear loss of modulation as the detection bandwidth increases.

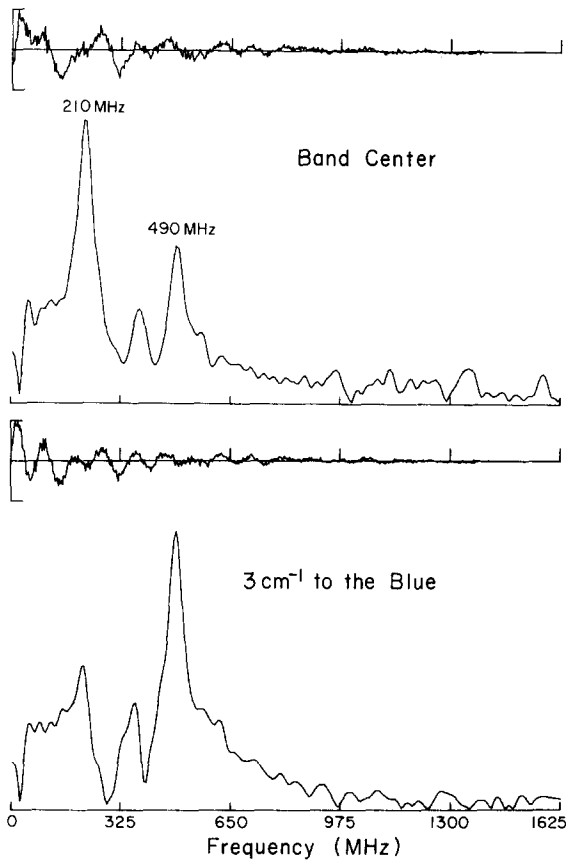

FIG. 8. Decay residuals and their Fourier transforms for excitation to two different portions of the 6_0^1 rotational contour and detection of the 1125 cm^{-1} dispersed fluorescence band. For both sets of data: $X = 3$ mm, $D = 100\ \mu$m, $P = 22$ psi He, BW = 0.4 Å, $R = 2.4$ Å, $T = 180$ °C.

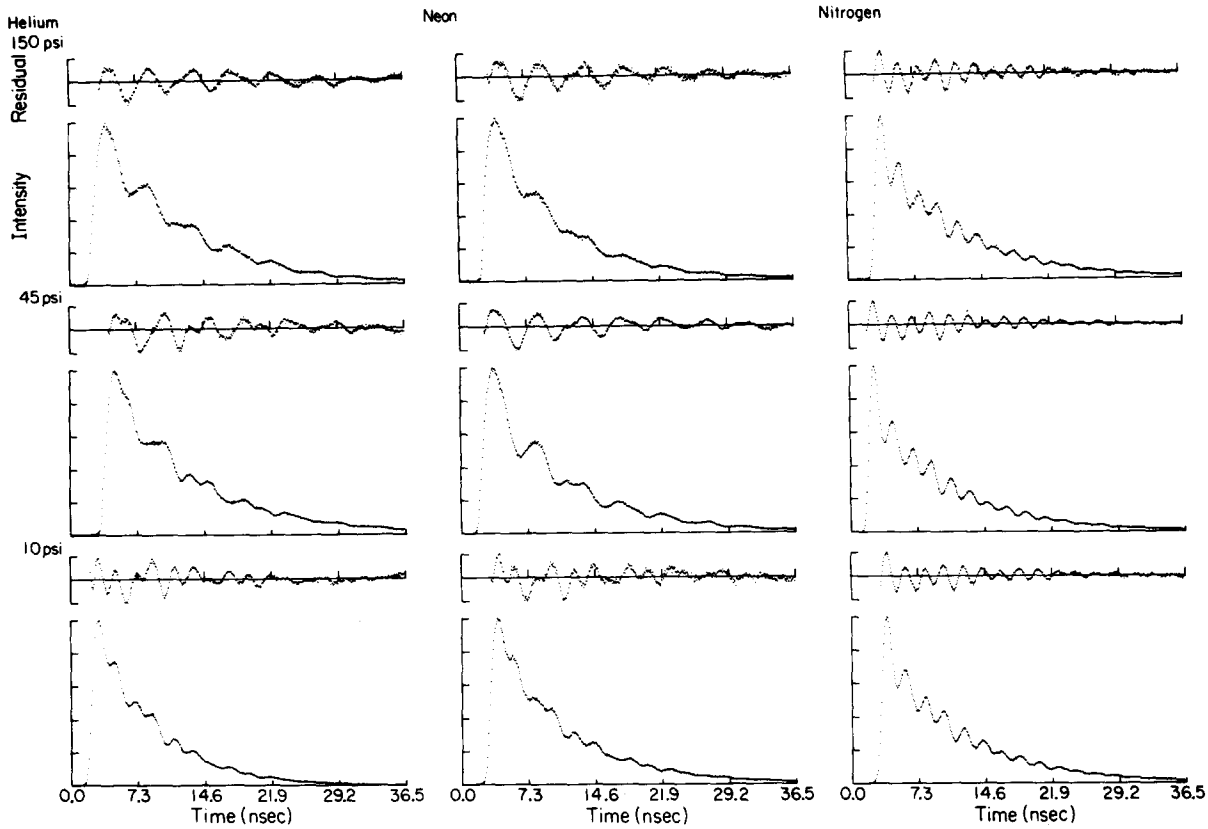

FIG. 9. Characteristic quantum beat patterns produced in helium, neon, and nitrogen expansions. The band detected is the 1125 cm^{-1} band. For all decays: $X = 5$ mm, $D = 150\,\mu$m, BW = 0.5 Å, $R \sim 1.6$ Å, $T = 180$ °C.

B. The influence of excitation wavelength

Using 3 cm^{-1} bandwidth excitation and exciting at various positions on the rotational contour[9] of the 1380 cm^{-1} band has revealed an excitation energy dependence to quantum beat patterns. This is clear from Fig. 8, in which the Fourier spectra of the beat patterns for different excitation wavelengths (λ_d = 1125 cm^{-1} band; 30 psi He expansion) change noticeably. Considering just the two most prominent Fourier components (210 and 490 MHz) one may note that excitation to the center of the rotational contour enhances the 210 MHz component relative to the 490 MHz one. Excitation at the blue edge of the band causes a relative increase in the 490 MHz component. (Although not shown in Fig. 8 similar behavior occurs for excitation to the red edge.) Although Fig. 8 was obtained for a helium expansion, similar trends have been found to apply to neon and nitrogen expansions as well.

C. Carrier gas effects

Figures 9 and 10 present fluorescence decays and Fourier transformed residuals of the 1125 cm^{-1} band as a function of carrier gas and carrier gas pressure. It is readily apparent that the relative intensities of the beat components change significantly for different expansion conditions. The 490 MHz component dominates for low pressures of He and Ne, and for all pressures of N_2. In contrast, the 210 MHz component only becomes most prominent at higher pressures of He and Ne. Given that both the 210 and 490 MHz Fourier components appear for all carrier gases used, it is unlikely that the trends shown in Figs. 9 and 10 are somehow linked with vibrationally hot species or van der Waals complexes. As will be seen in the next section, the changes are instead linked to changes in anthracene rotational temperature as expansion conditions vary.

In considering the results of Figs. 9 and 10, it is to be emphasized that the excitation bandwidth (~4 cm^{-1}) used to obtain the results is much narrower than that which was used (~20 cm^{-1}) to obtain the results of our previous communication.[1] In that work we reported the observation of relatively minor changes in beat patterns for comparable changes in carrier gas parameters.

D. Rotational envelopes

In an effort to determine the influence of molecular rotations on quantum beats in anthracene, excitation spectra have been taken with the nitrogen laser system across the rotational contour of the 6_0^1 band for various carrier gases and fluorescence detection wavelengths. Figure 11 presents the pertinent results. Although the spectra are not normalized to laser pulse energy, they all correspond to the same spectral range and their general features are quite reproducible. An obvious feature of all the spectra in the figure is the presence of a splitting of band shape. As discussed elsewhere,[9] this behavior is expected for transitions to an S_1–a_g

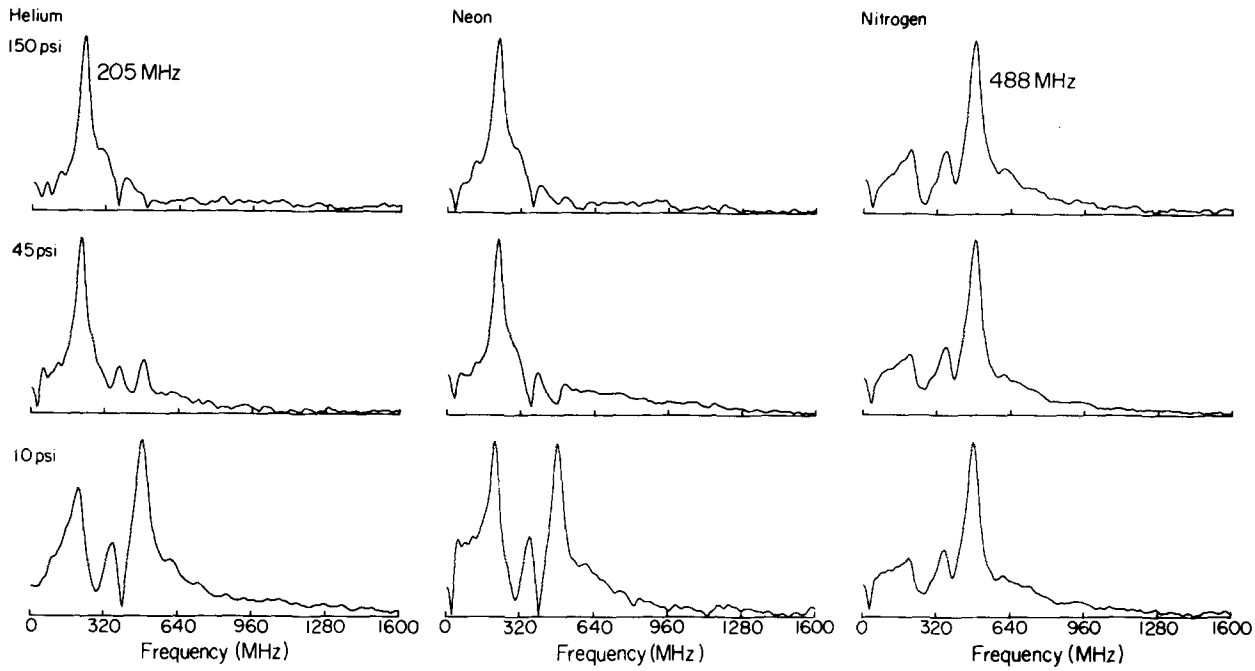

FIG. 10. The Fourier transformed residuals of the decays appearing in Fig. 9. Note the changes in the relative intensity of the various Fourier peaks.

vibrational level in anthracene (*B*-type band). As the carrier gas is changed from Ne to He to N_2, an apparent increase in splitting takes place and overall broadening occurs. Band contour calculations have linked these trends with an increased anthracene rotational temperature for N_2 relative to He and Ne expansions.[9]

Comparison of the spectra taken while selectively detecting the 1125 cm^{-1} (beating) band [Figs. 11(d)–11(f)] with those which were taken for detection of the 1459 cm^{-1} band [Figs. 11(a)–11(c)], and which appear essentially the same as spectra taken for total fluorescence detection, show that for given expansion conditions, the band structure is significantly broader, and the splitting larger for detection of the 1125 cm^{-1} band. The results indicate that the distribution of the rotational levels which give rise to beats is different than the overall distribution of rotational levels populated by the excitation process.

E. Phase-shifted quantum beats

The theoretical treatment of Sec. II B pertaining to the manifestations of vibration–vibration coupling in beat-modulated decays predicted the existence of 180° phase-shifted quantum beat patterns for selected dispersed fluorescence bands. Experimental observations clearly exhibiting such behavior have been reported[6] for anthracene excited to $S_1 + 1420\ cm^{-1}$. This has led us to attempt to observe such phase shifts in anthracene beats for 6^1(1380 cm^{-1}) excitation. Figure 12 presents a pair of decays at early time. The two were obtained under identical experimental conditions except for detection wavelength. One decay corresponds to detection of the 390 cm^{-1} dispersed fluorescence band, which exhibits very weakly modulated beats at 210 and 490 MHz (see Fig. 6). The other corresponds to detection of the 1125 cm^{-1} band, whose decay is more strongly modulated at these frequencies. The figure displays a clear shift of the 1125 cm^{-1} decay to later time than the 390 cm^{-1} decay. Similar shifts of the 1125 cm^{-1} decay also occur relative to decays of bands in the dispersed fluorescence spectra which are unmodulated. Comparison of calculated decays (see Sec. III G 2)

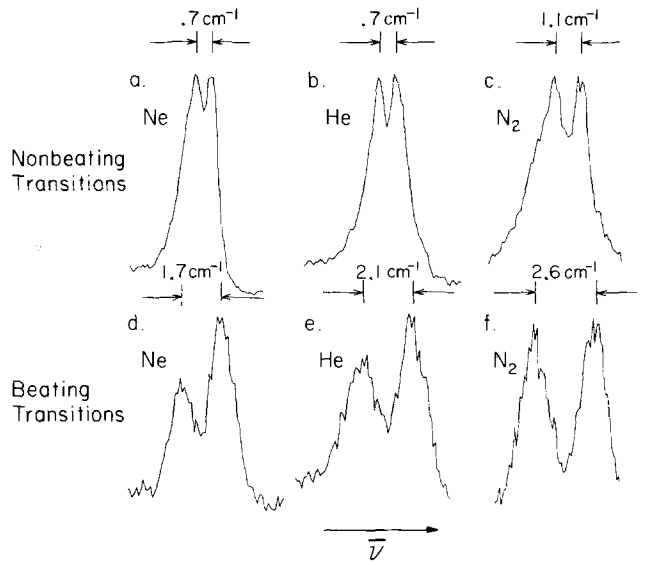

FIG. 11. Fluorescence excitation spectra taken with the nitrogen laser system and CW jet over the rotational contour of the 6_0^1 band for various detection and expansion conditions. The carrier gases used for the spectra are given in the figure. In all cases 25 psi pressure was used. The 'nonbeating" (Ref. 20) spectra [(a), (b), and (c)] correspond to detection of the intense dispersed fluorescence band at 1459 cm^{-1} ($R = 1.6$ Å). *These spectra do not noticeably change even as R becomes so large that essentially total fluorescence is collected.* The "beating" spectra [(d), (e), and (f)] correspond to detection of the 1125 cm^{-1} band ($R = 1.6$ Å). Although spectra are not normalized to laser power, the general features are very reproducible. For all spectra: $X = 3$ mm, $D = 100\ \mu$m, $T = 180$ °C.

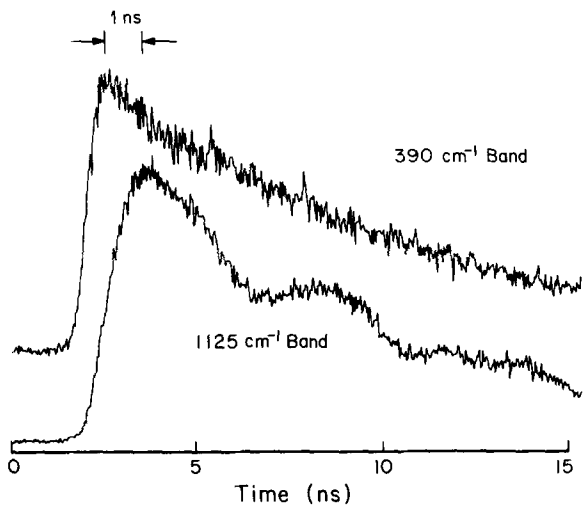

FIG. 12. Fluorescence decays of the 390 and 1125 cm^{-1} dispersed fluorescence bands of anthracene excited to 6^1. The decays were collected one directly after the other under identical conditions: $X = 3$ mm, $D = 100\ \mu m$, $P = 60$ psi He, BW = 0.5 Å, $R = 3.2$ Å, $T = 180$ °C. The shift of the 1125 cm^{-1} decay to later time is reproducible and also occurs for neon and nitrogen expansions. Although the decay of the 390 cm^{-1} band is weakly modulated (see Fig. 6), the modulation is not apparent in this figure due to noise.

with the experimental data reveal that the observed shift of the 1125 cm^{-1} decay is consistent with molecular decay functions of the form

$$G(t) \sim \left(1 - \sum_i a_i \cos \omega_i t\right) e^{-\Gamma t},$$

where all a_i's are > 0. The evidence, therefore, indicates that beat-modulated decays observed for the 1125 cm^{-1} band do, in fact, involve phase-shifted interference terms similar (but not as dramatic) to those observed for the 1420 cm^{-1} excitation.[6]

F. Magnetic field effects

The application of an external magnetic field to a molecule exhibiting quantum beats in its fluorescence decay might be expected to have a number of observable consequences,[3(b),4(a)] such as: (i) an effect on beat frequencies; (ii) an effect on the amplitudes of Fourier components associated with beats; and/or (iii) an effect on the characteristic relaxation rates of the states giving rise to the beats. The magnitude of such effects will depend on the strength with which the applied field couples to the beating states. Figure 13 presents beat-modulated fluorescence decays of anthracene taken under identical experimental conditions except for magnetic field parameters. Analysis of these decays reveals none (within experimental error) of the possible magnetic field effects listed above. On the other hand, the same field applied to pyrazine, a molecule known to undergo extensive singlet–triplet coupling,[22] shows a pronounced effect[4(a)] on the modulated decay of the S_1 vibrationless level, as also shown in Fig. 13.

G. Other anthracene beats and results on deuterated anthracenes

In the preceding discussion we have dealt exclusively with beats arising from 6^1-level excitation in h_{10}-anthracene.

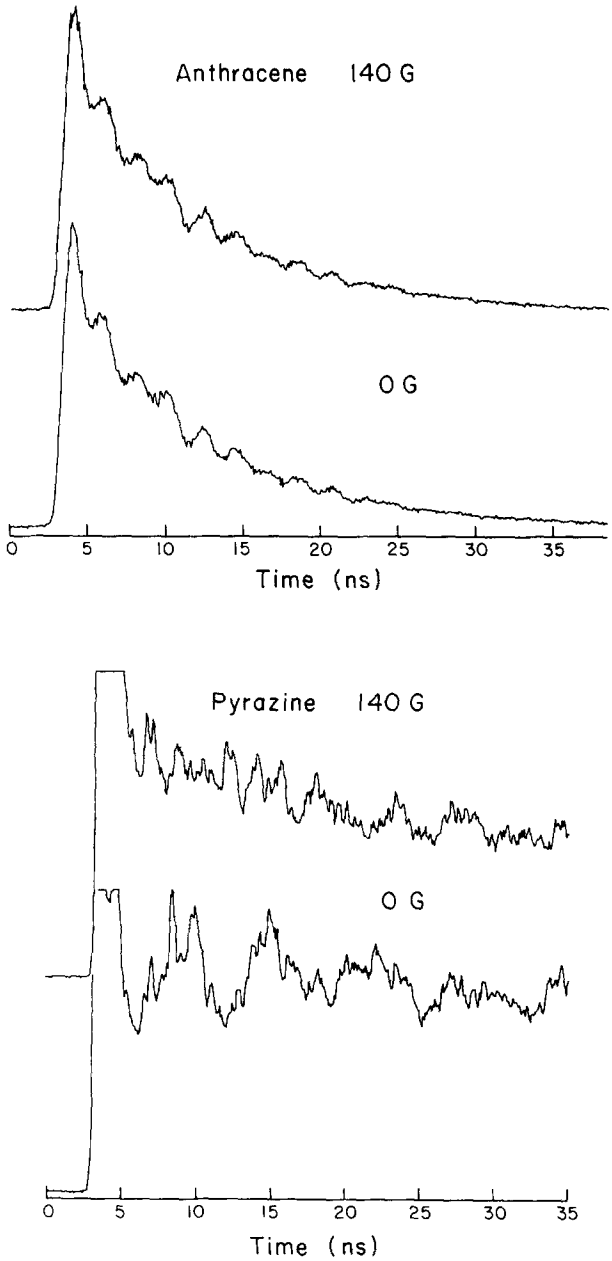

FIG. 13. A comparison of the effect of a static magnetic field on anthracene and pyrazine quantum beats. Decays were taken using the same experimental apparatus. For both anthracene decays excitation was to 6^1, the 1125 cm^{-1} was detected, $X = 3$ mm, $D = 100\ \mu m$, $P = 30$ psi N_2, BW = 0.4 Å, R 3.2 Å, and $T = 180$ °C. For the pyrazine decays the S_1-0^0 level was excited, the fluorescence band at ~590 cm^{-1} was detected, $X = 3$ mm, $D = 100\ \mu m$, $P = 40$ psi Ne, BW = 0.4 Å, $R = 16$ Å, and $T = 25$ °C. The pyrazine decays shown have been magnified along the intensity scale to better illustrate their differences.[4(a)]

It is pertinent to note that beats have been found for other excitations of h_{10}-anthracene, as well. For instance, for excitation at $S_1 + 1420$ cm^{-1}, very well-modulated decays arise.[6] The modulated decays for these excitations display sharp detection wavelength dependences and quantum beat phase shift behavior.

We have also studied the species $9d_1$-, $9,10d_2$-, and d_{10}-anthracene. However, quantum beats have not been observed for these species upon excitation of bands in the 1400 cm^{-1} region[9] of their S_1 manifolds when detecting at shifts of ~1125 cm^{-1} from the excitation energy. As a particular

example, Fig. 14 presents a comparison of dispersed fluorescence spectra for h_{10}-anthracene excited to $S_1 + 1380\ cm^{-1}$ (6_0^1) and d_{10}-anthracene excited to $S_1 + 1375\ cm^{-1}$. Although the spectra appear very similar, no beats have been observed for bands in the d_{10}-anthracene spectrum in the region corresponding to shifts from the excitation energy of $\sim 1125\ cm^{-1}$. It is possible that beats in the deuterated molecules will appear at different detection wavelengths. We are currently searching with increased time resolution for other beats in anthracene and anthracene derivatives. Very recent results[7] indicate that many of the bands in the 6^1 spectrum that do not show beats with 400 ps time resolution do show high frequency modulations (up to 8.5 GHz when 70 ps resolution is used.

V. DISCUSSION

To fully understand the implications that quantum beats in a given molecule have with regard to the intramolecular dynamical processes of that molecule, one must know the nature of the coupling which gives rise to the beats. Hence, in the first two sections to follow we discuss the evidence that links vibrational coupling within the S_1 manifold to anthracene beats. Following this, we consider the rotational level dependence of the beats. Finally, we discuss the ways in which anthracene quantum beats provide information relevant to the parameters associated with IVR processes.

A. Evidence against interelectronic state coupling

There are several reasons to reject interelectronic state coupling as an explanation for the quantum beats observed in anthracene. In the following we first present arguments against the involvement of S_1-triplet coupling. Next, S_1-singlet coupling is considered. Finally, we consider some of the evidence for intraelectronic state coupling.

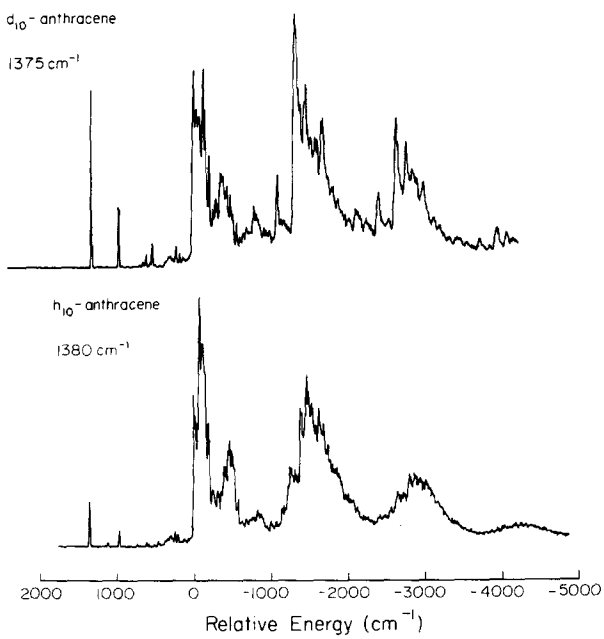

FIG. 14. A comparison of the dispersed fluorescence spectra of d_{10}-anthracene excited to $S_1 + 1375\ cm^{-1}$ and h_{10}-anthracene excited to $S_1 + 1380\ cm^{-1}$. For both spectra: $X = 5$ mm, $D = 150\ \mu m$, $P = 45$ psi N_2, $R = 1.6$ Å, and $T = 180$ °C.

Calculations[23] and experimental results[24] indicate that several triplet states have energies suitable to allow them to interact with the S_1–6^1 level and to produce mixed eigenstates which can give rise to beats. However, the lack of a dependence of anthracene beat parameters on applied magnetic fields, in contrast to the dramatic effects observed for other molecules which undergo singlet-triplet coupling[3(b),4(a)] (see Sec. IV) renders this coupling scheme improbable. Moreover, there are other reasons, which arise from the fact that triplet states are optically dark in absorption from *and* emission to S_0, to reject S_1-triplet coupling. (Note that these same arguments apply to S_1–S_0 coupling.) As was show in Sec. II B [case (1)], one consequence of a coupling between an optically active level and such dark levels is that *all* bands in the dispersed fluorescence spectrum are modulated in the same way and show exactly the same beat pattern. As a result, one need not spectrally resolve the fluorescence to observe beats.[3,4] This prediction is obviously inconsistent with our anthracene results. Furthermore, a singlet–triplet coupling scheme cannot account [see Eq. (4)] for quantum beat phase shifts such as have been observed for anthracene.

Calculations[23] also suggest that levels of the first $^1B_{3u}^-$ state of anthracene may be of the proper energy to couple to the 6^1 level of S_1 and give rise to beating states. (All other excited singlet states are too high in energy.) However, the $^1B_{3u}^-$ state is characterized by a vanishing oscillator strength connecting it to S_0.[23] The arguments presented above (based on the results of Sec. II B) to reject singlet–triplet mixing as an explanation for anthracene beats are valid here, as well. In addition, density of states considerations argue against the likelihood of significant S_1–$^1B_{3u}^-$ coupling at molecular energies corresponding to $S_1 + 1400\ cm^{-1}$ in anthracene. The energy of the $^1B_{3u}^-$ state is predicted[23] to greater than that of the $S_1(^1B_{2u}^+)$ state and, in fact, may be greater than $S_1 + 1400\ cm^{-1}$. Hence, the $^1B_{3u}^-$ level structure available for coupling with S_1 levels is more sparse than the level structure available within the S_1 manifold itself. The fact that a number of beating excitation bands occur in the $S_1 + 1400\ cm^{-1}$ region[6,7] argues against interactions with such a sparse manifold.

While there is no evidence to support the involvement of interelectronic state coupling in anthracene quantum beats, the existence of vibrational coupling within the S_1 manifold at $1380\ cm^{-1}$ is strongly suggested by the spectral results of the preceding paper.[21] There, it was shown that the SVL fluorescence spectrum for 6^1 excitation displayed characteristic manifestations of vibrational coupling within a discrete manifold of S_1 vibrational levels. This coincidence between intermediate case vibrational coupling and quantum beats seems more than fortuitous and is telling evidence regarding the coupling inteaction that gives rise to the beats. Moreover, one may note that the density of S_1 vibrational levels in this energy region is $\sim 25/cm^{-1}$. Therefore, the chance that one level will occur within several hundred MHz of the 6^1 level, with the proper symmetry, given vibrational

coupling symmetry restrictions, to interact with it, is large enough (several percent) that such a situation might reasonably be expected.

In brief summary, interelectronic state coupling is not a satisfactory explanation for the characteristics of anthracene beats. On the other hand, spectral evidence[21] implies that vibrational mixing within the S_1 manifold occurs for the 6^1 level and, therefore, is responsible for the beats. In the following section we present a discussion of phase shifts in anthracene beats which, perhaps, provide the most convincing evidence for the role that vibrational coupling plays in the beat phenomenon.

B. Vibrational coupling and quantum beat phase relationships in anthracene

As discussed in Ref. 6 and in Sec. II B of this paper, quantum beat phase relationships can be very useful in determining the coupling which gives rise to quantum interference phenomena in a particular molecule. For vibration–vibration coupling within an excited singlet manifold, one expects to see two types of beating decays, depending on the fluorescence band detected. These two types [case (2) and case (3) of Sec. II B] differ by 180° in the phases of the modulated portions of their decays, and also differ in the degree to which they are modulated. Clear observations of these manifestations of vibration–vibration coupling in anthracene excited to $S_1 + 1420$ cm^{-1} appear in Ref. 6.

The results of Fig. 12, which show a clear shift to later time of one beating decay relative to another for 6^1 excitation suggest that the beats corresponding to this excitation can be attributed to coupling between S_1 vibrational levels. The 1125 cm^{-1} decay, being the one shifted to later time ($-\cos \omega t$ modulation term) is assigned as a case (3)-type decay. The 390 cm^{-1} band is assigned as case (2). Consistent with these assignments is the fact that the modulation of the beats for the 390 cm^{-1} band is much less pronounced than that for the 1125 cm^{-1} band, as expected for case (2) vs case (3) bands.[6]

Having made the above case assignments, it is useful to ask if they are reasonable in terms of anthracene spectroscopy. The 390 cm^{-1} band can be assigned as $6_0^1 12_1^0$. On the other hand, the 1125 cm^{-1} band *cannot* be readily assigned as a band of the form $6_n^1 A_m^0$, where A is some known optically active mode or combination of such modes[9,21] Spectroscopic considerations therefore, imply that the 390 cm^{-1} band derives its emission strength from the same zero-order vibrational level that carries the absorption strength, while the 1125 cm^{-1} band derives its strength from a vibrational level $\{X\}^{\{n\}}$, different from 6^1. Given coupling between 6^1 and $\{X\}^{\{n\}}$, the 390 cm^{-1} band is *expected* to be case (2) and the 1125 cm^{-1} band, case (3). It is consistent with these considerations that the decay of the 6_0^1 band has a modulation depth similar to the $6_0^1 12_1^0$ band (Fig. 6), and that the bands corresponding to $1125 + n \times 390$ cm^{-1} are modulated in similar fashion to the 1125 cm^{-1} band (despite spectral congestion). One may note that because the progression $1125 + n \times 390$ cm^{-1} continues to $n = 3$, it is probable that the level $\{X\}^{\{n\}}$ is of the form $\{Y\}^{\{m\}} 12^1$, and that the 1125 cm^{-1} transition may be represented as $\{Y\}_{\{m\}}^{\{m\}} 12_0^1$. Given the excited state value for the 12 fundamental (385 cm^{-1}) and the requirement that $\{X\}^{\{n\}}$ be nearly resonant with 6^1, this implies an excited state value of 995 cm^{-1} for $\{Y\}^{\{m\}}$.

In closing this section, it is appropriate to point out that we have made the above analysis in terms of a two level theory. Of course, such an analysis is a simplification for a large molecule like anthracene. As mentioned in Sec. II C multilevel systems may be expected to give rise to beat-modulated decays with characteristics somewhat different than those arising from two-level systems. These differences explain some of the discrepancies between the experimental results and the two-level predictions of Sec. II B. For instance, as will be explicitly discussed below, the existence of a number of beat frequencies in the experimental decays may be attributed to coupling dependent on rotational level. Also, the less than complete modulation of the 1125 cm^{-1} band may be explained in numerous ways in terms of multilevel effects.[25] Finally, the fact that bands with unmodulated decays[20] are observed in the same spectrum as bands that show beating decays may be attributed to the coupling of levels to 6^1 which either give rise to unresolvably high frequency beat components, or give rise to such a large number of beat frequencies that any modulations wash out. [See note added in proof.]

C. Rotational level dependence of anthracene quantum beats

Three categories of experimental results presented in this paper are pertinent to the rotational level dependence of beats in anthracene. All are consistent in their implications. The carrier gas effect on the beat pattern (Figs. 9 and 10), in light of the effect of carrier gas on rotational cooling in anthracene,[9] suggests that the 490 MHz beat component arises in jets for which the rotational temperature is relatively high, whereas the 210 MHz component dominates at low rotational temperature. [Note that we consider only these two components since one or the other (or both) is the major component in any modulated decay observed.] From this it can be said that the 490 MHz component is associated with higher energy rotational levels than is the 210 MHz component. This point is supported by the fact that, for a given set of expansion conditions, the observed beat pattern is strongly dependent upon that part of the rotational contour excited by the picosecond laser (Fig. 8). Excitation to low J, K_a excited state levels at the center of the rotational contour favors the 210 MHz component, while excitation to the blue or red edges of the contour, which populates higher energy J, K_a levels, results in an increase in the 490 MHz contribution. Finally, the excitation spectra of Fig. 11 show that for expansion conditions favoring the 210 MHz component, the rotational contours corresponding to excitation of beating states [Figs. 11(d) and 11(e)] are narrower, with smaller splittings than is the contour observed under conditions favorable to the 490 MHz component [Fig. 11(f)]. Clearly, then, there is a rotational level dependence to the beats, with the higher frequency component arising, in general, from levels of higher J, K_a than the lower frequency component.

Besides the dependence of beat pattern on rotational level, the spectra of Fig. 11 also indicate that the distribution

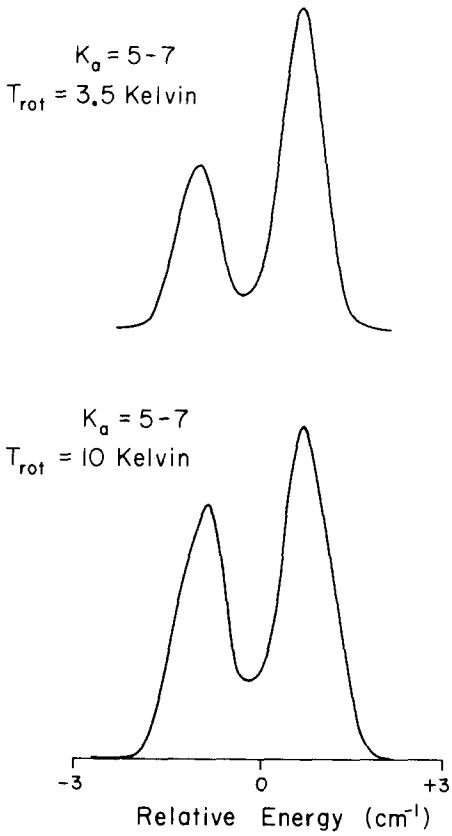

FIG. 15. *B*-type rotational contours of h_{10}-anthracene at two rotational temperatures calculated by only allowing transitions to excited state K_a values of 5 to 7. Allowed J values were 0 to 30. The calculations were performed to better understand the differences in observed rotational contours of the 6^1 band (*B* type, see Ref. 9) for different fluorescence detection wavelengths and expansion conditions (Fig. 11).

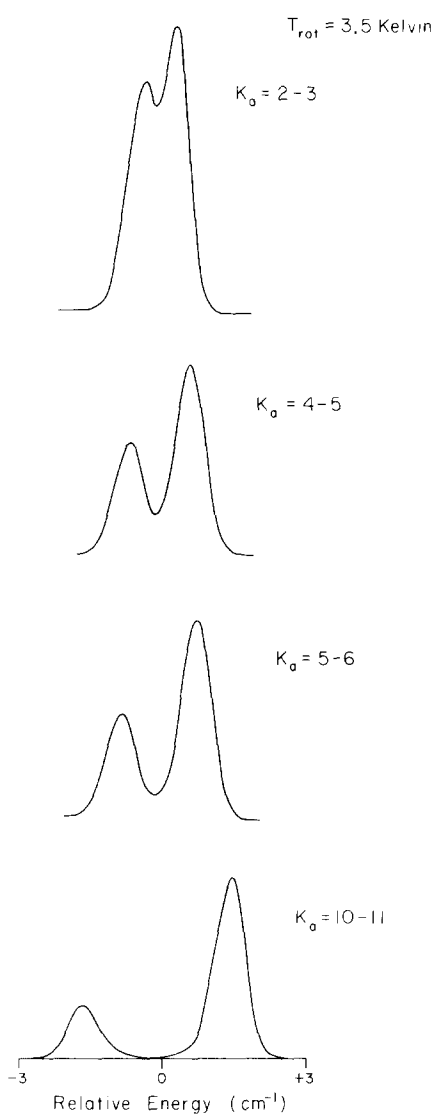

FIG. 16. *B*-type rotational contours of h_{10}-anthracene at a rotational temperature of 3.5 K for various ranges of allowed excited state K_a values. J values of 0 to 30 were allowed.

of rotational levels involved in beats at either 210 or 490 MHz ($\lambda_d = 1125\ cm^{-1}$) correspond to higher average J, K_a values than the distribution of rotational levels populated as a whole by the exciting light [compare Figs. 11(a) to 11(d), 11(b) to 11(e), and 11(c) to 11(f)]. This is an important result. It strongly emphasizes the role that rotational level structure plays in the coupling which gives rise to the 1125 cm^{-1} emission band and the beats. One can get an idea of the J, K_a values associated with the beating states by comparing the spectra of Fig. 11 with the results of band contour calculations. We have made such calculations using the program cited in a previous paper,[9] and have included an option whereby the values of excited state J and K_a values can be restricted. Calculated results appear in Figs. 15–17. We have taken the rotational temperature to be 3.5 K for most of the calculated spectra, since that value seems to fit the He and Ne spectra for λ_d = "total fluorescence" [Figs. 11(a) and 11(b)]. One result that emerges from a comparison of the upper spectrum of Fig. 15 with Figs. 11(d) and 11(e) is that restricting the permissible values of K_a can account for the shape and splittings of the observed rotational contours. One can also account in this way for the appearance of the nitrogen contour [Fig. 11(f)] by assuming an increased (10 K) rotational temperature (Fig. 15). A limited study of the K_a-range dependence of the calculated spectra has been performed (Fig. 16). It is evident from the figure that the spectra are quite sensitive to the lower value of K_a chosen. On the other hand, increasing the upper limit of K_a to include up to five allowed values has a relatively minor effect (not shown in Fig. 16) on calculated band shapes. Regarding our interpretation of the observed spectra, the calculated results imply that levels with $K_a \lesssim 4$ are not extensively involved in the coupling which gives rise to the 1125 cm^{-1} beating band. In contrast to the calculated results for limited K_a, Fig. 17 shows that the calculated spectra for limited J are not as successful in matching the observed spectra for any of the J ranges tried. Moreover, considering the trend of the figure, it does not appear that a reasonable J range will do so.

Having deduced a rotational level dependence to anthracene beats from experimental and calculated results, it is appropriate to ask if vibrational coupling schemes based on Fermi resonance or Coriolis coupling can account for the form of this dependence. Unfortunately, any detailed attempts to fit theory to experiment are extremely complicated owing to the large number of unknown parameters that exist (e.g., precise rotational constants, coupling matrix elements, etc.). However, it is useful to note that Fermi resonance, as

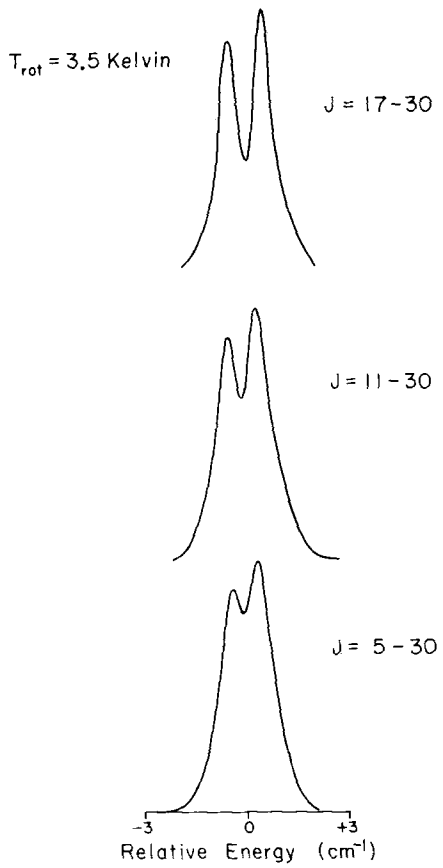

FIG. 17. *B*-type absorption rotational contours of h_{10}-anthracene at a rotational temperature of 3.5 K for various ranges of all allowed excited state J values. All possible K_a values were allowed.

well as Coriolis coupling interactions, can be dependent on rotational level. For Coriolis coupling such a dependence is obvious since the coupling matrix element is J, K_a dependent.[26] In Fermi resonance, the matrix element is constant with rotational level, but the zero-order energy spacings and hence the coupling between coupled rotational levels in the two manifolds may vary due to differences in the rotational constants of the two vibrational states.[7]

D. Quantum beats IVR in anthracene

In Sec. II D we have considered the relation of IVR processes to the quantum beats which might arise from vibrational coupling. In as much as the quantum interference effects in anthracene closely fit expected manifestations of vibrational coupling, it is appropriate to view anthracene beats in terms of an IVR process. (Specifically, for instance, one may regard the 1125 cm^{-1} band as being an example of collisionless vibrationally "relaxed" fluorescence, with the phase shift of its decay being regarded in terms of a characteristic relaxation time.) Doing so, one may note several points regarding the parameters associated with IVR in this large molecule. Firstly, in the 1400 cm^{-1} region of the S_1 vibrational level structure of the molecule, IVR is present but *restricted* in extent.[6] In this regard, it is pertinent to note that excitations to this same region produce dispersed fluorescence spectra[21] which display manifestations of limited vibrational coupling. Secondly, coupling matrix elements on the order of 0.01 cm^{-1} (i.e., on the order of observed beat frequencies), leading to characteristic redistribution times in the nanoseconds, could strongly influence IVR processes in the molecule. Finally, IVR processes could be extremely sensitive to rotational level. The rotational level dependence of the anthracene beats corresponding to 6^1 excitation is direct evidence for this sensitivity.

Note added in proof: With the recent acquisition of a fast detection system, we have significantly enhanced the temporal resolution of our apparatus to the point that it can now resolve quantum beats at least as fast as 11 GHz and a decay as short as ~10 ps. New results on anthracene using this system have been obtained which are very significant to this molecule's dynamics in general and to the results reported in this paper in particular. We have now observed beat modulated delays for all prominent excitation bands in the range E_{vib} = 1380–1800 cm^{-1}. Fast beats (3.6, 4.9, 8.5 GHz) consistent with the manifestations of multilevel vibrational coupling at E_{vib} = 1380 cm^{-1} have been observed [Phys. Rev. Lett. (in press)]. Results which show the transition from restricted to dissipative IVR (τ_{IVR} ~75 ps) have been reported [Chem. Phys. Lett. (in press)]. And, finally, more results showing the effect of rotational structure on vibrational quantum beats have been obtained.

ACKNOWLEDGMENT

It is a pleasure to acknowledge the support of this work by the National Science Foundation.

[1]Wm. R. Lambert, P. M. Felker, and A. H. Zewail, J. Chem. Phys. **75**, 5958 (1981).
[2]See, for example, S. Haroche, in *High Resolution Laser Spectroscopy*, edited by K. Shimoda (Springer, New York, 1976), p. 254.
[3](a) J. Chaiken, M. Gurnick, and J. D. McDonald, Chem. Phys. Lett. **61**, 197 (1979); J. Chem. Phys. **74**, 106 (1981). (b) H. Henke, H. L. Selzle, T. R. Hays, S.H. Lin, and E. W. Schlag, Chem. Phys. Lett. **77**, 448 (1981).
[4](a) P. M. Felker, Wm. R. Lambert, and A. H. Zewail, Chem. Phys. Lett. **89**, 309 (1982); (b) W. Sharfin, M. Ivanco, and S. C. Wallace, J. Chem. Phys. **76**, 2095 (1982); (c) S. Okajima, H. Saigusa, and E. C. Lim, *ibid.* **76**, 2096 (1982); (d) B. J. van der Meer, H. Th. Jonkman, G. M. ter Horst, and J. Kommandeur, *ibid.* **76**, 2099 (1982); (e) M. Ivanco, J. Hager, W. Sharfin, and S. C. Wallace, *ibid.* **78**, 6531 (1983).
[5]M. Bixon, J. Jortner, and Y. Dothan, Mol. Phys. **17**, 109 (1969).
[6]P. M. Felker and A. H. Zewail, Chem. Phys. Lett. **102**, 113 (1983).
[7]P. M. Felker and A . H. Zewail (to be published); see also note added in proof.
[8]J. L. Charlton and R. Agagnier, Can. J. Chem. **51**, 1852 (1973).
[9]W. R. Lambert, P. M. Felker, J. A. Syage, and A. H. Zewail, J. Chem. Phys. **81**, 2195 (1984).
[10]D. P. Millar and A. H. Zewail, Chem. Phys. **72**, 381 (1982).
[11]G. R. Hansen, B. W. Wallin, and F. E. Lytle, Rev. Sci. Instrum. **50**, 64 (1979).
[12]E. F. Zalewski, R. A. Keller, and R. Engleman, Jr., J. Chem. Phys. **70**, 1015 (1979), and references therein.
[13]J. A. Syage, P. M. Felker, and A. H. Zewail, J. Chem. Phys. **81**, 2233 (1984).
[14](a) D. W. Marquardt, J. Soc. Indian Appl. Math. **11**, 431 (1963); (b) P. R. Bevington, *Data Reduction and Error Analysis for the Physical Sciences* (McGraw–Hill, New York, 1969).
[15](a) A. Grinvald, Anal. Biochem. **75**, 260 (1976); (b) A. Grinvald and I. Z. Steinberg, *ibid.* **59**, 583 (1974).
[16](a) E. O. Brigham, *The Fast Fourier Transform* (Prentice–Hall, Englewood Cliffs, NJ, 1974); (b) J. W. Cooley and J. W. Tukey, Math. Comput. **19**, 297 (1965).
[17]R. B. Blackman and J. W. Tukey, *The Measurement of Power Spectra* (Dover, New York, 1958).

[18]C. K. Yuen and D. Fraser, *Digital Signal Analysis* (Pittman, London, 1979).

[19]The assignment of bands is dealt with in a previous paper (Ref. 9). The notation follows that of Brand, Collomon, and Watson. For example, $6_0^1 12_1^0$ indicates a transition from the 1380 cm^{-1} level (the sixth highest energy a_g mode) to one quantum of the 390 cm^{-1} mode (the 12th highest energy a_g mode). It should be mentioned that our discussion of the beats does not depend crucially on the assignment of the 1380 cm^{-1} band and we use it primarily as a convenient label.

[20]Of course, "nonbeating" must be qualified in that the time resolution of our experimental system only allows the observation of beat frequency components less than ~ 2 GHz. Recent work using increased time resolution (~ 70 ps response function) indicates that many bands in the 6^1 spectrum do, in fact, exhibit decays which are modulated at high frequencies (as high as 8.5 GHz). This work will be published shortly. (See note added in proof.)

[21]W. R.Lambert, P. M. Felker, and A. H. Zewail, J. Chem. Phys. **81**, 2209 (1984).

[22]For example, Refs. 4(a), 4(c), and 4(d), and references therein.

[23]R. Pariser, J. Chem. Phys. **24**, 250 (1956).

[24]U. Laor, J. C. Hsieh, and P. K. Ludwig, Chem. Phys. Lett. **22**, 150 (1973).

[25]Note that there are other likely *experimental* causes for the less than 100% modulation observed for the decay of the 1125 cm^{-1} band. Among these experimental influences is the inability to isolate beating bands from nonbeating (Ref. 20) bands because of finite monochromator resolution.

[26]E. B. Wilson, J. Chem. Phys. **4**, 313 (1936).